Inorganic Chemistry
Article
pubs.acs.org/IC

Phosphite as Polyanion-Based Cathode for Li-Ion Battery: Synthesis, Structure, and Electrochemistry of LiFe(HPO$_3$)$_2$

Hooman Yaghoobnejad Asl and Amitava Choudhury*

Department of Chemistry, Missouri University of Science and Technology, Rolla, Missouri 65409, United States

Supporting Information

ABSTRACT: A new lithium containing iron(III) phosphite, LiFe(HPO$_3$)$_2$, has been synthesized via a solvent-free, low temperature, solid-state synthesis route. The crystal structure of this material has been determined employing single-crystal X-ray diffraction, which indicates that the compound has a three-dimensional structure formed by isolated FeO$_6$ octahedral units joined together via bridging HPO$_3$ pseudopyramidal moieties. This arrangement leads to the formation of channels along all the three crystallographic directions, where channels along the *a*- and *b*-axes host Li$^+$ ions. The compound was further characterized by TGA, IR, and Mössbauer spectroscopic techniques. Additionally, it has been demonstrated that this phase is electrochemically active toward reversible intercalation of Li$^+$ ions and thus can be used as a cathode material in Li-ion cells. An average discharge potential of 2.8 V and a practical capacity of 70 mAh·g^{-1} has been achieved as indicated by the results of cyclic voltammetry and galvanostatic charge−discharge tests.

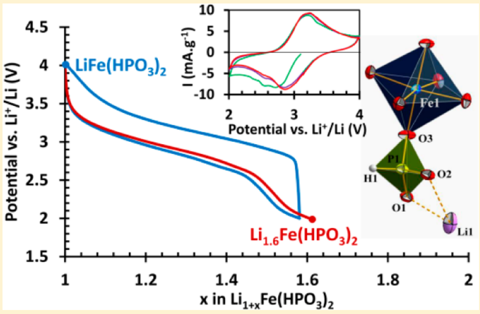

INTRODUCTION

In today's world, there are plenty of avenues of applications where Li-ion battery has been envisaged as a prime source of energy storage or power supply.[1−4] For all the applications, safety is the primary concern, but different qualities of batteries are sought after based on whether the application is focused on mobile or stationary devices. For example, a battery for vehicular application has to be high in energy density, while for smart grid application, a low cost, long cycle life and fast charge−discharge battery will take precedence over the high energy density.[5] Thus, one may expect to have different materials in Li-ion battery to fulfill different requirements of applications, and in this race cathode component merits most attention because it determines the voltage and the specific capacity.

In this respect, polyanion compounds of the transition metals are being actively investigated as cathode materials for Li-ion batteries.[6,7] Because of the strong covalent bonding between the main group element in the center of the polyhedron and oxygen atoms in the polyanion moiety, the oxygen atoms are held tightly in the structure. This imparts structural stability to the compound and chances of oxygen release upon charging to high potentials are minimized, thus improving the safety features of the cathode. Moreover, by changing the electronegativity of the central atom in a polyanion one can vary the iono-covalency of the metal−ligand bond in X−O−M (X = B, S, P, Si etc.; M = transition metal) linkage through the inductive effect of X, thereby tuning the redox potential on the transition metal center.[8] This ability of tuning redox potential makes polyanion chemistry unique when compared to pure oxides. Another feature of this polyanion chemistry is the propensity of forming a wide variety of two-dimensional (2-D) and three-dimensional (3-D) structures through different types of connectivity between the polyanion and the transition metals.[9] These structures are stabilized under different synthetic conditions as employed by chemists.[10]

In this context, various compounds of transition metals have been synthesized incorporating PO$_4^{3-}$,[7,11] SO$_4^{2-}$,[12−14] SiO$_4^{4-}$,[15,16] BO$_3^{3-}$,[17,18] mixed PO$_4^{3-}$, and CO$_3^{2-}$,[19,20] etc. Among the various newly discovered polyanion cathodes, triplite, LiFeSO$_4$F (3.9 V), is emerging as a strong contender of cathode for Li-ion battery,[21] challenging the most outstanding polyanion cathode, olivine LiFePO$_4$.[11]

Despite the enormous efforts devoted toward polyanion compounds for their electrochemical properties, phosphite-based compounds received little or no attention. The only example was that of Rojo et al., showing very small electrochemical activity in Li$_{1.43}$[Fe$_{4.43}^{II}$Fe$_{0.57}^{III}$(HPO$_3$)$_6$]-1.5H$_2$O with a specific capacity of 12 mAh·g^{-1}.[22] Recently, we have shown that a new phosphite polyanion based material, Li$_3$Fe$_2$(HPO$_3$)$_3$Cl, is electrochemically active with a practical specific capacity of 70 mAh·g^{-1} (theoretically 131.4 mAh·g^{-1}) and an average discharge voltage above 3.0 V.[23] The relatively high voltage observed for this compound can be assigned to the inductive effects of the phosphite and chloride groups coordinated to the iron center.

With the above encouraging results, we have focused more on the synthesis and electrochemical activity of other possible phosphite-based compounds of iron. In this article, we report

Received: April 20, 2015
Published: June 19, 2015

DOI: 10.1021/acs.inorgchem.5b00900
Inorg. Chem. 2015, 54, 6566−6572

Table 1. Crystal Data and Structure Refinement Parameters for $LiFe(HPO_3)_2$

empirical formula	$LiFe(HPO_3)_2$	Z	8
formula wt ($g \cdot mol^{-1}$)	222.75	ρ_{calc} ($g \cdot cm^{-3}$)	2.644
crystal system	tetragonal	$F(000)$	872
space group	$I\bar{4}2d$	temperature (K)	298(2)
a (Å)	10.593(6)	GOF on F^2	1.159
b (Å)	10.593(6)	R [$I > 2\sigma(I)$]	$R_1 = 0.0250$
c (Å)	9.971(4)		$wR_2 = 0.0675$
$\alpha = \beta = \gamma$ (deg)	90	R [all data]	$R_1 = 0.0259$
V (Å^3)	1119.0(3)		$wR_2 = 0.0679$

Table 2. Atomic Coordinates and Equivalent Isotropic Displacement Parameters of the Atoms (U_{eq} = 1/3rd of the Trace of the Orthogonalized U Tensor)

atom	Wyckoff	site	occ.	x/a	y/b	z/c	U_{eq} [Å^2]
Fe1	8d	0.2.	1	0.2819(1)	0.2500	0.1250	0.008(1)
P1	16e	1	1	0.4463(1)	0.2511(1)	0.4013(1)	0.011(1)
O1	16e	1	1	0.3444(2)	0.1902(2)	0.4886(2)	0.014(1)
O2	16e	1	1	0.4259(2)	0.2121(2)	0.2543(2)	0.013(1)
O3	16e	1	1	0.5774(2)	0.2164(3)	0.4483(2)	0.015(1)
Li1	8d	0.2.	1	0.5627(8)	0.2500	0.1250	0.024(2)
H1	16e	1	1	0.4440(4)	0.3736(2)	0.4090(4)	0.007(1)

for the first time the synthesis and structural details of a new lithium iron(III) phosphite, $LiFe(HPO_3)_2$, and demonstrate its activity toward reversible intercalation of Li^+ ions. This new phase has a theoretical capacity 120.3 $mAh \cdot g^{-1}$ and exhibits extremely good capacity retention upon successive cycling.

EXPERIMENTAL SECTION

Materials. γ-Fe_2O_3 (99+% metal basis) was purchased from Alfa Aesar, $LiOH \cdot H_2O$ (98% reagent grade) and H_3PO_3 (98% extra pure) were obtained from Acros Organics. All the chemicals were used as received without further purification.

Synthesis. First, 0.80 g of γ-Fe_2O_3 (5 mmol), 0.94 g of $LiOH \cdot H_2O$ (23 mmol), and 2.46 g of H_3PO_3 (30 mmol) were mixed and ground in an agate mortar pestle, and the resulting high viscosity paste was then transferred to a Teflon cup. The cup was then closed with a Teflon cap, placed in a stainless steel Paar reaction vessel, and heated for 7 days in an oven at 150 °C. After removal from the oven, the reaction vessel was allowed to cool down to room temperature, and the product, which composed of uniform small clear crystals, was washed with hot water followed by filtration to remove the unreacted reagents and dried overnight in open air.

Single-Crystal X-ray Diffraction. Crystal structure of $LiFe(HPO_3)_2$ was solved from single-crystal intensity data sets collected on a Bruker Smart Apex diffractometer with monochromated Mo Kα radiation (λ = 0.7107 Å). A suitable crystal was selected and mounted on a glass fiber using epoxy-based glue. The data were collected using SMART[24] software at 298 K employing a scan of 0.3° in ω with an exposure time of 10 s/frame. The cell refinement and data reduction were carried out with SAINT,[25] while the program SADABS[25] was used for the absorption correction. The structure was solved by direct methods using SHELX-97[26] and difference Fourier syntheses. Full-matrix least-squares refinement against $|F^2|$ was carried out using the SHELXTL-PLUS[26] suit of programs. The structure of $LiFe(HPO_3)_2$ was solved in tetragonal system in a noncentrosymmetric space group, $I\bar{4}2d$. The electron densities of Fe, P, and O atoms were located from Fourier difference maps and refined isotropically. Subsequently, electron density for the Li^+ ion appeared at a distance of 2 Å from the oxygen atoms. An anisotropic refinement performed on the located atoms revealed one more electron density peak, approximately 1.2 Å away from the phosphorus atom. The latter has been assigned as the phosphite hydrogen and subsequently refined isotropically after adding soft constrains to fix P–H bond distance close to the theoretical value. Details of the final refinement and crystallographic information for $LiFe(HPO_3)_2$ is provided in Table 1. The fractional atomic coordinates along with the isotropic thermal displacement parameters are given in Table 2. Selected interatomic distances are listed in Table 3.

Table 3. Selected Bond Lengths for $LiFe(HPO_3)_2$[a]

bonds	distances (Å)	bonds	distances (Å)
Fe1–O3 $\times 2^{\#1}$	1.969(2)	P1–O3	1.511(2)
Fe1–O1 $\times 2^{\#2,\#3}$	2.010(3)	P1–H1	1.299(2)
Fe1–O2 $\times 2^{\#4,\#5}$	2.037(2)	Li1–O1 $\times 2^{\#8}$	2.026(6)
P1–O1	1.529(3)	Li1–O2 $\times 2^{\#6,\#7}$	1.982(7)
P1–O2	1.539(2)		

[a] #1: x +0, $-y$ +1/2, $-z$ + 1/4. #2: $-y$, x, $-z$. #3: $-y$ +0, $-x$ +1/2, z +1/4. #4: y +1/2, $-x$ + 1/2, $-z$ + 1/2. #5: y +1/2, x, z −1/4. #6: $-y$ +1/2, x −1/2, $-z$ +1/2. #7: $-y$ +1/2, $-x$, z −1/4. #8: x +0, $-y$ −1/2, $-z$ +1/4.

Powder X-ray Diffraction. For assessing the sample purity, powder XRD pattern of the as synthesized product was collected on a PANalytical X'Pert Pro diffractometer equipped with a Cu $K_{\alpha_{1,2}}$ anode and a linear array PIXcel detector over a 2θ range of 5–90° with an average scanning rate of 0.025° s. The acquired pattern was then subjected to quantitative phase analysis via the Rietveld method using the single-crystal structure solution as the starting model for $LiFe(HPO_3)_2$ to calculate the amount of impurity phase(s).

Mössbauer Spectroscopy. First, 75 mg of the as prepared sample was mounted on a Pb sample holder and subjected to analysis by ^{57}Fe Mössbauer spectroscopy at room temperature using a constant acceleration spectrometer in transmission geometry. The spectrometer was equipped with a ^{57}Co (50 mCi) gamma-ray source embedded in Rh matrix and calibrated for isomer shift with respect to a standard α-Fe foil at room temperature. The collected experimental data were then fitted to Lorentzian function using the Recoil software.[27]

Thermogravimetric Analysis (TGA). TGA has been done on about 15 mg of manually separated crystals of pure $LiFe(HPO_3)_2$ using a TA Instruments Q50 TGA in a temperature range of 25–800 °C with a scan rate of 10 $°C.min^{-1}$ under nitrogen flow.

IR Spectroscopy. The IR spectrum was collected using Thermo Nicolet Nexus 470 FT-IR spectrometer over 500–4000 cm^{-1} on manually separated pure sample embedded in KBr pellet.

Electrochemical Testing. For electrochemical studies of $LiFe(HPO_3)_2$, a cathode film was prepared. In this regard, the active material, $LiFe(HPO_3)_2$, was first milled with super P conductive carbon vigorously in a SPEX 8000 miller for 2 h followed by addition of poly vinylidene fluoride (PVDF) as binder dissolved in *N*-methyl-2-pyrrolidone (NMP). The resulting mixture was further ball milled for 20 min until a homogeneous, viscous slurry was obtained. The ratio of the active material, conducting carbon, and the binder in cathode mix was 65:25:10. The cathode mix was then spread as a film of uniform thickness onto a flat sheet of aluminum current collector with a glass rod and dried in a vacuum oven for 12 h at 80 °C. The milled cathode mix was also tested for structural stability by powder X-ray diffraction, and the XRD pattern clearly showed the retention of the crystal structure during the cathode mix preparation (Supporting Information, Figure S1). The SEM images of the pulverized (ball-milled) sample mixed with carbon after 2 h of milling are presented in the Supporting Information (Figure S2). The sizes of the particles as estimated from the SEM images range from submicrometer particulates to particles of several micrometers in diameters. However, the size distribution of the majority of particles is approximately in the range 2−5 μm in diameter.

For electrochemical tests, CR2032 type coin cells were fabricated using the above composite cathode film cut into circular disks (3/8 in. diameter) with 5.0−6.0 mg of active material loading. The cells were assembled in an argon filled glovebox with oxygen concentration below 2.0 ppm. The cathode disk and Li anode (0.75 mm thickness Li ribbon cut into circular disk) were mounted in the cell using a Celgard 2325 circular sheet placed between the two electrodes as the separator. The electrolyte, 1 M solution of $LiPF_6$ in DMC-EC (1:1) was then added and the cell was sealed with a coin cell crimper. The prepared cells were aged for equilibration for several hours before electrochemical testing.

Cyclic voltammograms were obtained using a PAR EG&G potentiostat/galvanostat model 273 in the potential range of 2.0−4.0 V (vs Li^+/Li) with a scan rate of 0.05 $mV{\cdot}s^{-1}$. Voltage-composition profiles were obtained using galvanostatic charge−discharge experiments on an Arbin Instruments battery tester, model BT2043, in the potential range 2.0−4.0 V with a constant current charge and discharge modes at various C-rates.

■ RESULTS AND DISCUSSION

Synthesis. The initial ratio of the reactants had a crucial role on the percentage yield of the major product and identity of the byproducts formed in this reaction. It has been found that the highest purity of $LiFe(HPO_3)_2$ could be obtained when Fe_2O_3:$LiOH{\cdot}H_2O$:H_3PO_3 were mixed in 1:4:6:6 molar ratio, with $Fe_2(HPO_3)_3$ as the only major impurity phase. Ratios of acid to base greater than the above increases the $Fe_2(HPO_3)_3$ mass fraction in the final product while smaller ratios yield an unknown impurity phase (Supporting Information, Figure S3). A quantitative phase analysis via Rietveld refinement performed on the reaction products obtained under optimized conditions revealed that the product contained 85% $LiFe(HPO_3)_2$ and 15% $Fe_2(HPO_3)_3$ by mass, as demonstrated in Figure 1. It is to be noted here that ex situ time-dependent PXRD evolution of the reaction product(s) indicated that the optimized synthesis of 85% $LiFe(HPO_3)_2$ and 15% $Fe_2(HPO_3)_3$ can be achieved in 72 h. In fact, $LiFe(HPO_3)_2$ as the major product can be formed during the first 6 h of the synthesis, and further heating was required to remove/reduce the intensity of impurity peaks (Supporting Information, Figure S4). However, 7 days of reaction was required to grow crystals suitable for single-crystal X-ray diffraction. Because the identity of the impurity phase was known, this sample was used for electrochemical studies rather than the one with unknown impurities (Supporting Information, Figure S3).

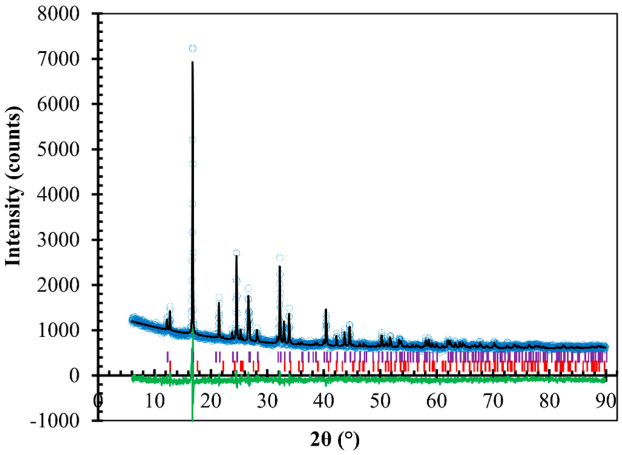

Figure 1. Rietveld refinement on the powder XRD of the as-synthesized product. Open circles, observed intensity; black line, calculated intensity; green line, difference curve; diffraction position indicator, $LiFe(HPO_3)_{2}$–, purple tick mark; $Fe_2(HPO_3)_{3}$–, red tick mark.

Crystal Structural Description. $LiFe(HPO_3)_2$ is a three-dimensional open-framework structure made from vertex-shared FeO_6 octahedra and HPO_3 pseudopyramidal units incorporating Li-ions within its channels. The structure of $LiFe(HPO_3)_2$ is isostructural to a recently published vanadium analogue, $LiV(HPO_3)_2$.[28] The asymmetric unit of $LiFe(HPO_3)_2$ contains six non-hydrogen atoms and one hydrogen atom (Figure 2a). There is one crystallographically distinct iron center, located at the special position, 8*d*, and adopts an octahedral coordination with oxygen atoms from phosphite groups. The Fe−O distances fall in the range 1.969(2)−2.037(2) Å, which agree well with the reported Fe^{3+}−O bond lengths.[29] The phosphorus of the phosphite group is in +3 oxidation state and bonded to three oxygen atoms and one hydrogen atom in a distorted tetrahedral (or pseudopyramidal) unit. The P−O distances are in the range 1.511(2)−1.539(2) Å and the P−H bond length is 1.29(4) Å (constrained), all corroborating well with the reported values for P−O and P−H distances in many reported metal phosphites.[22,29,30] The Li atom is located in the special position, 8*d*, and is coordinated by

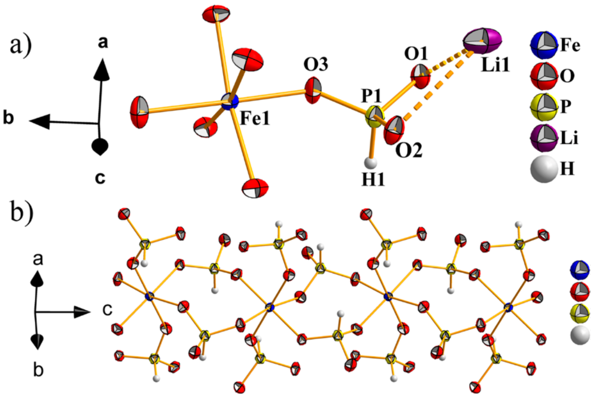

Figure 2. Connectivity pattern and coordination spheres of atoms in $LiFe(HPO_3)_2$ as obtained from single-crystal X-ray structure solution. Thermal ellipsoids are given at 80% probability. Only atoms present in the asymmetric unit are labeled (a); connectivity pattern of FeO_6 and HPO_3 units along the *c*-axis (b).

DOI: 10.1021/acs.inorgchem.5b00900
Inorg. Chem. 2015, 54, 6566−6572

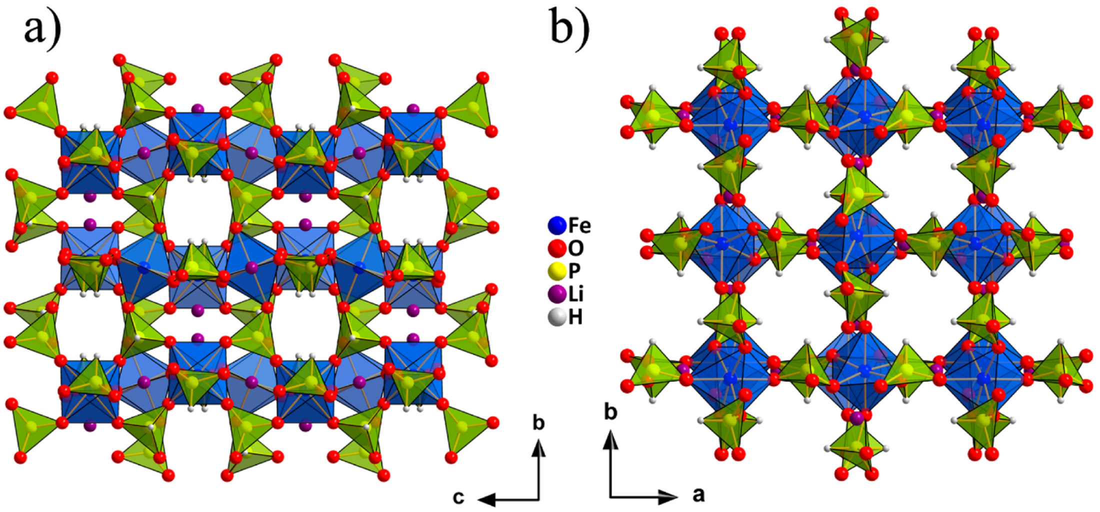

Figure 3. Perspective view of the packing diagram of the crystal structure of $LiFe(HPO_3)_2$ as viewed along the *a*-axis (a) and *c*-axis (b). Blue, FeO_6 octahedra; green, HPO_3 pseudo pyramidal units.

four oxygen atoms (from two crystallographically distinct O atoms) in an irregular nonplanar geometry with Li1−O1 and Li1−O2 bond lengths of 2.026(6) and 1.982(7) Å, respectively. The results of the bond valence sum calculations (BVS)[31] for Fe1 (BVS = 3.09) and P1 (BVS = 3.97, disregarding hydrogen) confirms the oxidation states Fe and P as 3+. It is to be noted that the proof of oxidation state of +3 for P in phosphite group from BVS value is indirect because of the lack of reliable bond valence parameters for pure P(III)−O bonds.[32] The BVS calculation actually represents the oxidation state of $(PH)^{4+}$ group rather than P in HPO_3 moiety as also noted by Rojo et al. in an iron phosphite compound.[29]

Each Fe atom makes six Fe−O−P linkages and similarly each P atom makes three P−O−Fe linkages. Thus, the crystal structure is composed of strictly alternating FeO_6 octahedra and HPO_3 units sharing vertices. The vertex linking polyhedra form four-membered rings (connecting only P and Fe atoms) through the two bridging HPO_3 units between the two FeO_6 octahedra; these four-membered rings are further corner-shared along the *c*-axis to form a chain (Figure 2b). These chains are further connected through HPO_3 units laterally along *a*- and *b*-axes, creating interconnected channels in all three crystallographic directions (Figure 3). Two types of channels are formed when viewed along the *a*- or *b*-axes. Li^+ ions can be seen occupying the slightly elongated zigzag channels, while the straight hexagonal-shaped channels are left empty. On the other hand, channels along the *c*-axis are also empty and have larger diameter formed by the eight-membered ring, and the hydrogen atoms of the phosphite moiety are protruding into the channel. It is to be noted here that Li-ions prefer the channels where inner walls are exclusively built by oxygen atoms.

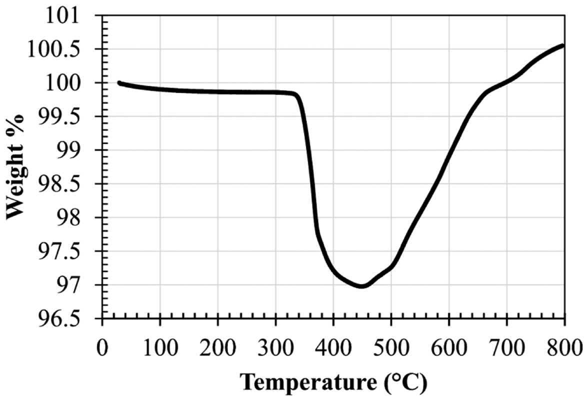

Figure 4. TGA curve for $LiFe(HPO_3)_2$.

Thermogravimetric and Spectroscopic Characterization. The TGA plot of the pure sample exhibits an initial mass loss of 0.15% up to a temperature of 300 °C, which can be assigned to the removal of adsorbed moisture (Figure 4). The structure remains stable up to 320 °C, after which it loses 3% of its mass, indicating the decomposition of the delicate HPO_3 groups. As the temperature increases from 450 to 800 °C, a considerable mass gain can be observed, which can be assigned to the oxidation of P(III) to P(V) to form a phosphate or pyrophosphate as a result of oxygen impurity in the N_2 purge gas, similar to other phosphite based materials reported in the literature.[22,33]

Figure 5 depicts the FT-IR spectrum of $LiFe(HPO_3)_2$. The spectrum is composed of the signature sharp P−H stretching mode at 2450 cm^{-1} and the P−O stretching modes prevailing in the region 900−1100 cm^{-1} overlapping with the bending vibrations of P−H bond.[22] The low frequency part of the spectrum shows moderate absorption peaks assigned to the bending modes of P−O bonds. The absence of strong absorption peaks in the 3200−3500 cm^{-1} region indicates

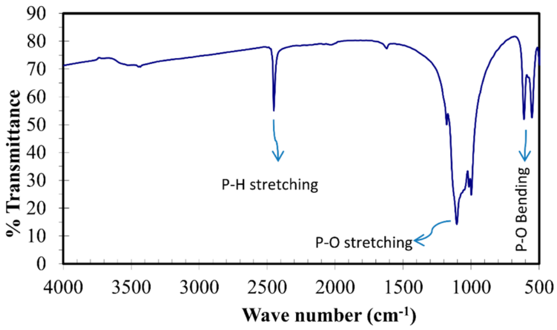

Figure 5. FT-IR spectrum of $LiFe(HPO_3)_2$.

that the P−H bond is preserved during the synthesis and there is no sign of oxidation of P−H bond to P−O−H.

The Mössbauer spectrum of the as-synthesized product is given in Figure 6 and the isomer shift (IS) and quadrupole splitting (QS) parameters derived from the curve fitting are given in Table 4. The observed spectrum has been fitted with two quadrupolar doublets, consistent with the results of powder XRD, with each doublet representing one crystallographically distinct Fe(III) in octahedral coordination as in $LiFe(HPO_3)_2$ and $Fe_2(HPO_3)_3$, respectively. Site population analysis as obtained through the Lorentzian fit suggests that $LiFe(HPO_3)_2$ and $Fe_2(HPO_3)_3$ each contributes 87 and 13% to the area, respectively, corroborating well with the quantitative phase analysis results achieved via powder XRD refinement. The IS values are consistent with Fe(III) ions in octahedral coordination.[34] The Mössbauer spectrum also rules out the existence of other iron containing impurity species as evident from the spectra collected over the velocity range from −8.5 to +8.5 $mm \cdot s^{-1}$.

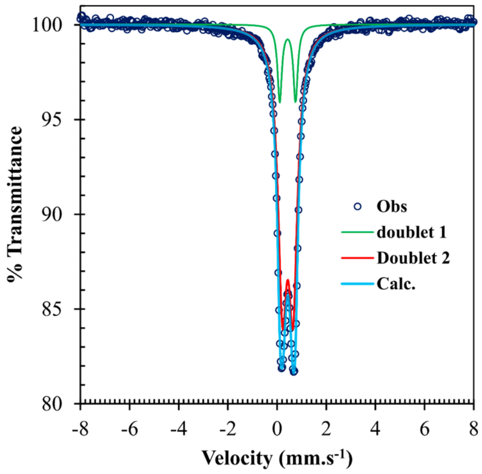

Figure 6. Mössbauer spectrum of the as-synthesized product, $LiFe(HPO_3)_2$ (85%) and $Fe_2(HPO_3)_3$ (15%).

Table 4. Lorentzian Deconvolution Fit Parameters of the Mössbauer Spectrum

	IS ($mm \cdot s^{-1}$)	QS ($mm \cdot s^{-1}$)	site population
doublet 1	0.429 (2)	0.644(2)	12.9(7)
doublet 2	0.434(6)	0.431(1)	87.1(7)

Electrochemistry. To evaluate the basic electrochemical properties of the prepared composite cathode, cyclic voltammetry (CV) tests were performed on the coin cells (Figure 7) which demonstrate that the phase is active with respect to Li intercalation/deintercalation. The cell exhibits an initial open circuit potential of 3.1 V upon scanning to the potential of 2.0 V. The reductive lithiation peak for $LiFe(HPO_3)_2$ appears at 2.71 V, with a weak shoulder at 2.5 assigned to the reduction of $Fe_2(HPO_3)_3$ phase. On reversing the scan toward 4.0 V, the corresponding oxidative delithiation peak can be observed at 3.22 V. Repeating the cycling shows two obvious events: first, a shift in the $LiFe(HPO_3)_2$ reduction peak toward more positive direction (2.86 V), indicating an increase in the cell discharge potential; and second, decrease in $Fe_2(HPO_3)_3$ phase reduction current. Additional cycling reveals that the position of oxidation and reduction peaks for $LiFe(HPO_3)_2$ do not shift any more and the magnitude of the cathodic and anodic currents at the peak potentials is very reproducible, evidencing the high reversibility of the redox process.

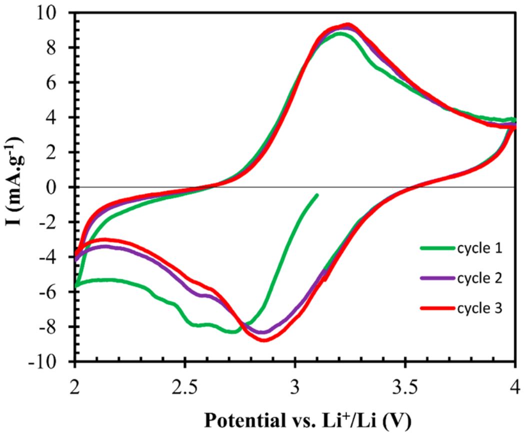

Figure 7. Cyclic voltammograms of the composite cathode with respect to Li^+/Li. Cathodic current is negative.

The galvanostatic charge−discharge curves at C/50 rate for the $LiFe(HPO_3)_2$ phase at room temperature and 40 °C are shown in Figure 8. To assess the contribution of the $Fe_2(HPO_3)_3$ impurity phase toward the total discharge capacity, coin cells of pure $Fe_2(HPO_3)_3$ phase was fabricated in the same manner and the specific discharge capacity was found to be negligible and also rapidly decaying with cycling. Therefore, the observed specific capacity can be assigned to the active $LiFe(HPO_3)_2$ phase reliably, albeit corrections were made to account for the inactive/less-active mass of the $Fe_2(HPO_3)_3$ phase in the composite cathode mix.

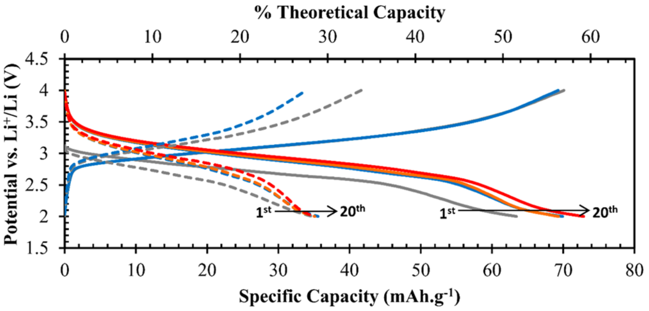

Figure 8. C/50 voltage-composition profiles of $LiFe(HPO_3)_2$. Dotted line, room temperature; solid line, 40 °C; gray, 1st; blue, 2nd; orange, 3rd; red, 20th cycles.

As the iron center in $LiFe(HPO_3)_2$ is in +3 oxidation state, the as-fabricated cells are already in charged state. The cells were initially subjected to discharge by reductive lithiation at room temperature (dotted lines) shows sloppy voltage profiles, indicating solid-solution formation between the oxidized and reduced phases. At this condition, the discharge terminates after insertion of 0.3 Li^+ ion per formula unit (36 $mAh \cdot g^{-1}$). Repeating the test at 40 °C, however, shows considerable improvement in capacity achievement with intercalation of 0.6 Li^+ ion per formula unit (72 $mAh \cdot g^{-1}$), revealing the existence of polarization effects which can be thermally activated. Such findings suggest that the limited achievable capacity may be due to the poor electronic and/or ionic conductivity of the material, which can be improved by reducing the particle size and applying more efficient carbon coating procedures.

The first discharge curve for both room temperature and 40 °C cycled cells starts from the open circuit potential, 3.1 V, while for the subsequent cycles, the discharge starts at a higher potential of 3.4 V vs Li^+/Li redox couple, in agreement with the cyclic voltammetry results. In addition, Li^+ intercalation for $LiFe(HPO_3)_2$ during the discharge occurs at an average potential of 2.82 V, which stands higher than some phosphate based materials, e.g., fluoro tavorite $LiFePO_4F$.[35,36]

Despite the limited capacity achievement, $LiFe(HPO_3)_2$ exhibit outstanding capacity retention when cycled at different C-rates for prolonged amounts of time (Figure 9). The cell cycled at 40 °C exhibits a steady specific capacity of about 70 $mAh{\cdot}g^{-1}$ during the first five cycles at C/50. Increasing the C-rate to C/20 causes a corresponding decrease in the specific capacity by 15 $mAh{\cdot}g^{-1}$. Further increase in discharge rate to C/10 and C/5 reduces the specific capacity to 50 and 43 $mAh{\cdot}g^{-1}$, respectively. However, returning the discharge rate back to C/50 recovers the original value of 70 $mAh{\cdot}g^{-1}$, indicating that the drop in capacity at higher C-rates is reversible and associated with different polarization mechanism inside the cell.

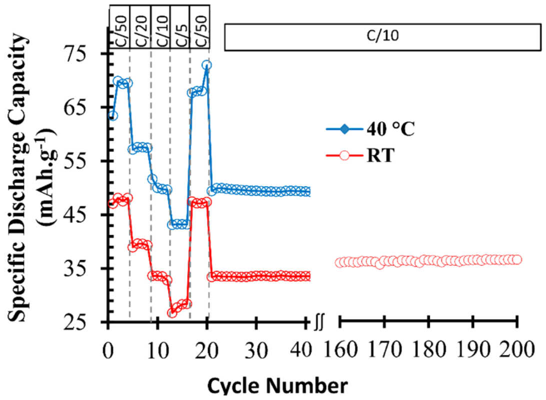

Figure 9. Capacity retention at various C-rates for $LiFe(HPO_3)_2$ cathode.

As expected the cell cycled at 40 °C shows higher specific capacity for all C-rates, but for both systems virtually no capacity fading can be detected even after 200 cycles. These results indicate the stability of $LiFe(HPO_3)_2$ crystal structure and the reversible nature of Li^+ ion intercalation. The retention of the structural integrity after electrochemical cycling has been confirmed by ex situ XRD of the reduced cathode material retrieved after breaking the button cell (Supporting Information, Figure S5). However, it was not possible to refine the powder pattern or locate the position of the inserted Li-ion due to the poor quality of the diffraction data. The excellent capacity retention may be related to the three-dimensional interconnected channels of the crystal structure. It is well-known that cathode materials where Li^+ diffusion is restricted to 1-D channels, for example, in olivine $LiMPO_4$ (M = Fe and Mn), are susceptible to blockage of Li^+ diffusion path due to defects and impurities.[37] This blockage eventually causes capacity fading and reduced cycle-life. This problem is less likely to occur in materials with 3-D interconnected network of ionic diffusion paths and thus capable of showing good cycling stability as in the case of tavorite.[38]

■ CONCLUSIONS

In this Article, we demonstrated that a novel phosphite with iron, the most abundant and environmentally benign transition metal, $LiFe(HPO_3)_2$, can be synthesized in a solvent-less low temperature synthesis route. The phase has been shown to be electrochemically active for reversible intercalation of Li^+ ions, with an average discharge voltage of 2.8 V and an experimental capacity of about 70 $mAh{\cdot}g^{-1}$, has been achieved at 40 °C. Simple synthesis, low cost materials, and excellent capacity retention of this phase may find applications where energy density is not a concern.

■ ASSOCIATED CONTENT

Ⓢ Supporting Information

X-ray crystallographic data for compound, $LiFe(HPO_3)_2$, in CIF format, PXRD patterns of (i) ball-milled sample with carbon, (ii) sample with the unknown impurity, (iii) discharged cathode (reductively lithiated) and (iv) time-dependent evolution of synthesis products as well as the SEM images of ball milled sample. The Supporting Information is available free of charge on the ACS Publications website at DOI: 10.1021/acs.inorgchem.5b00900.

■ AUTHOR INFORMATION

Corresponding Author

*E-mail: choudhurya@mst.edu.

Notes

The authors declare no competing financial interest.

■ ACKNOWLEDGMENTS

We acknowledge the funding from Materials Research Centre (Missouri S&T) and University of Missouri Research Board. We are also grateful to Professors Nick Leventis and Pericles Stavropoulos for the donation of a potentiostat and a glovebox, respectively.

■ REFERENCES

(1) Whittingham, M. S. *Chem. Rev.* **2004**, *104*, 4271−4302.
(2) Armand, M.; Tarascon, J.-M. *Nature* **2008**, *451*, 652−657.
(3) Dunn, B.; Kamath, H.; Tarascon, J.-M. *Science* **2011**, *334*, 928−935.
(4) Larcher, D.; Tarascon, J.-M. *Nature Chem.* **2014**, *7*, 19−29.
(5) Yang, Z.; Zhang, J.; Kintner-Meyer, M. C. W.; Lu, X.; Choi, D.; Lemmon, J. P.; Liu, J. *Chem. Rev.* **2011**, *111*, 3577−3613.
(6) Ellis, B.; Lee, K. T.; Nazar, L. F. *Chem. Mater.* **2010**, *22*, 691−714.
(7) Masquelier, C.; Croguennec, L. *Chem. Rev.* **2013**, *113*, 6552−6591.
(8) Padhi, A. K.; Manivannan, V.; Goodenough, J. B. *J. Electrochem. Soc.* **1998**, *145*, 1518−1520.
(9) Murugavel, R.; Choudhury, A.; Walawalkar, M. G.; Pothiraja, R.; Rao, C. N. R. *Chem. Rev.* **2008**, *108*, 3549−3655.
(10) Tarascon, J.-M.; Recham, N.; Armand, M.; Chotard, J.-N.; Barpanda, P.; Walker, W.; Dupont, L. *Chem. Mater.* **2010**, *22*, 724−739.
(11) Padhi, A. K.; Nanjundaswamy, K. S.; Goodenough, J. B. *J. Electrochem. Soc.* **1997**, *144*, 1188−1194.
(12) Anji Reddy, M.; Pralong, V.; Caignaert, V.; Varadaraju, U. V.; Raveau, B. *Electrochem. Commun.* **2009**, *11*, 1807−1810.
(13) Recham, N.; Chotard, J.-N.; Dupont, L.; Delacourt, C.; Walker, W.; Armand, M.; Tarascon, J.-M. *Nature Mater.* **2010**, *9*, 68−74.
(14) Rousse, G.; Tarascon, J.-M. *Chem. Mater.* **2014**, *26*, 394−406.
(15) Nytén, A.; Abouimrane, A.; Armand, M.; Gustafsson, T.; Thomas, J. O. *Electrochem. Commun.* **2005**, *7*, 156−160.

(16) Islam, M. S.; Dominko, R.; Masquelier, C.; Sirisopanaporn, C.; Armstrong, A. R.; Bruce, P. G. *J. Mater. Chem.* **2011**, *21*, 9811−9818.

(17) Legagneur, V.; An, Y.; Mosbah, A.; Portal, R.; Le Gal La Salle, A.; Verbaere, A.; Guyomard, D.; Piffard, Y. *Solid State Ionics* **2001**, *139*, 37−46.

(18) Yamada, A.; Iwane, N.; Harada, Y.; Nishimura, Sh.-I; Koyama, Y.; Tanaka, I. *Adv. Mater.* **2010**, *22*, 3583−3587.

(19) Chen, H.; Hautier, G.; Ceder, G. *J. Am. Chem. Soc.* **2012**, *134*, 19619−19627.

(20) Chen, H.; Hao, Q.; Zivkovic, O.; Hautier, G.; Du, L.; Tang, Y.; Hu, Y.; Ma, X.; Grey, C. P.; Ceder, G. *Chem. Mater.* **2013**, *25*, 2777−2786.

(21) Barpanda, P.; Ati, M.; Melot, B. C.; Rousse, G.; Chotard, J.-N.; Doublet, M.-L.; Sougrati, M. T.; Corr, S. A.; Jumas, J.-C.; Tarascon, J.-M. *Nature Mater.* **2011**, *10*, 772−779.

(22) Chung, U.; Mesa, J. L.; Pizarro, J. L.; de Meatza, I.; Bengoechea, M.; Fernandez, J. R.; Arriortua, M. I.; Rojo, T. *Chem. Mater.* **2011**, *23*, 4317−4330.

(23) Yaghoobnejad Asl, H.; Ghosh, K.; Vidal Meza, M. P.; Choudhury, A. *J. Mater. Chem. A* **2015**, *3*, 7488−7497.

(24) *Bruker-SMART*; Bruker AXS Inc.: Madison, Wisconsin, 2002.

(25) *Bruker-SAINT and SADABS*; Bruker AXS Inc.: Madison, Wisconsin, 2008.

(26) Sheldrick, G. M. *Acta Crystallogr., Sect. A: Found. Crystallogr.* **2008**, *A64*, 112−122.

(27) Recoil software: Lagarec, K.; Rancourt, D. G. *Phys. Res. B* **1997**, *129*, 266−280.

(28) Huang, H.-L.; Huang, S.-H.; Lai, C.-W.; Wu, J.-R.; Lii, K.-H.; Wang, S.-L. *J. Chin. Chem. Soc.* **2013**, *60*, 691−694.

(29) Chung, U.-C.; Mesa, J. L.; Pizarro, J. L.; Fernández, J. R.; Marcos, J. S.; Garitaonandia, J. S.; Arriortua, M. I.; Rojo, T. *Inorg. Chem.* **2006**, *45*, 8965−8972.

(30) Chung, U.; Mesa, J. L.; Pizarro, J. L.; Jubera, V.; Lezama, L.; Arriortua, M. I.; Rojo, T. *J. Solid State Chem.* **2005**, *178*, 2913−2921.

(31) Brown, I. D.; Altermatt, D. *Acta Crystallogr., Sect. B: Struct. Sci.* **1985**, *B41*, 244−247.

(32) Loub, J. *Acta Crystallogr., Sect. B: Struct. Sci.* **1991**, *B47*, 468−473.

(33) Hamchaoui, F.; Alonzo, V.; Venegas-Yazigi, D.; Rebbah, H.; Fur, E. L. *J. Solid State Chem.* **2013**, *198*, 295−302.

(34) Menil, F. *J. Phys. Chem. Solids* **1985**, *46*, 763−789.

(35) Ellis, B. L.; Ramesh, T. N.; Rowan-Weetaluktuk, W. N.; Ryan, D. H.; Nazar, L. F. *J. Mater. Chem.* **2012**, *22*, 4759−4766.

(36) Yaghoobnejad Asl, H.; Choudhury, A. *RSC Adv.* **2014**, *4*, 37691−37700.

(37) Morgan, D.; Van der Ven, A.; Ceder, G. *Electrochem. Solid-State Lett.* **2004**, *7*, A30−A32.

(38) Ramesh, T. N.; Lee, K. T.; Ellis, B. L.; Nazar, L. F. *Electrochem. Solid-State Lett.* **2010**, *13*, A43−A47.